752, June 1978.
[53] T. L. Hierl, J. J. Berenz, and S. I. Long, "GaAs pulsed Read IMPATT diodes," in *Proc. 6th Biennial Cornell Eng. Conf.*, pp. 211–219, Aug. 1977.
[54] Available from Nippon Electric Co.
[55] M. Omori, F. Rosztoczy, and R. Hayashi, "X-band GaAs double-drift IMPATT devices," *Proc. IEEE*, vol. 61, pp. 255–256, Feb. 1973.
[56] J. A. Rupp, private communication.

# High-Frequency Limitations of IMPATT, MITATT, and TUNNETT Mode Devices

MICHAEL E. ELTA, MEMBER, IEEE, AND GEORGE I. HADDAD, FELLOW, IEEE

*Invited Paper*

***Abstract*—High-frequency limitations of IMPATT and other mode devices are explored by concentrating on the details of the large-signal injected current pulse formation. Simple waveform models are given for injected current pulses of large widths, and various scaling relations are also included. The large-signal injected current pulse is calculated by use of a modified Read equation where attention is given to the effect of the intrinsic response time and the tunneling current. The poor high-frequency performance of GaAs devices is explained by postulating that the intrinsic response time is larger than expected. Tunneling current is shown to increase the high-frequency performance of GaAs diodes. Device efficiencies are calculated for specific diode structures by using a computer simulation which includes mixed avalanche-tunnel breakdown. The results for GaAs and Si devices are given, and the results are discussed and compared.**

## I. INTRODUCTION

MANY REASONS have been given for the high-frequency limitations of IMPATT mode devices such as package effects, series resistance, and skin effects [1] which cause the match between the device and circuit to become increasingly difficult for high-frequency operation. Diffusion-aided spreading of the injected current pulse [2], [3] can also limit the performance of IMPATT mode devices at very high frequencies, and the diffusion can also affect the intrinsic buildup of the injected current pulse [4]. The saturation of the ionization rates at high electric fields [5] will cause a decrease in the device efficiency at high frequencies. Thermal considerations are also important to high-frequency operation of these devices [6]. This paper will concentrate on the details of the injected current pulse formation and show how the pulsewidth is affected by device parameters, material parameters, and frequency. This effect is believed to be the major reason why GaAs IMPATT mode devices have had little experimental success in achieving oscillation in the low millimeter-wave frequency range. GaAs IMPATT mode devices have been built at 50 GHz with good efficiencies [7]. Si mode devices have achieved oscillation in a harmonic mode up to 423 GHz [8] and in a fundamental mode up to 341 GHz [9]. The limit of Si devices to near 400 GHz is probably due to a combination of the previously mentioned effects. The effect of tunneling current on the high-frequency performance is also discussed. Mixed avalanche-tunnel breakdown in semiconductors [10]–[13] and its effect on transit-time devices [14]–[18] has been discussed elsewhere.

The purpose of this paper is to discuss some fundamental high-frequency limitations of IMPATT mode devices where tunneling is also considered. Simple waveform models are given for injected current pulses of large widths, and various scaling relations are also included. The large-signal injected current pulse is calculated by use of a modified Read equation. Device efficiencies are calculated by using a computer simulation which includes mixed tunnel-avalanche breakdown. The results for GaAs and Si devices are given and compared. Three distinct modes of operation are identified for different widths of the generation region. These include the normal IMPATT mode, the MITATT (*mi*xed-*t*unneling-*a*valanche *t*ransit-*t*ime) mode, where both tunneling and avalanche break-

Manuscript received July 6, 1978; revised November 7, 1978. This work was supported by the Air Force Office of Scientific Research, Air Force Systems Command USAF, under Grant AFOSR-76-2939B.

M. E. Elta was with the Department of Electrical and Computer Engineering, Electron Physics Laboratory, University of Michigan, Ann Arbor, MI 48109. He is now with Lincoln Laboratory, Massachusetts Institute of Technology, Lexington, MA 02173.

G. I. Haddad is with the Department of Electrical and Computer Engineering, Electron Physics Laboratory, University of Michigan, Ann Arbor, MI 48109.

0018-9480/79/0500-0442$00.75 ©1979 IEEE

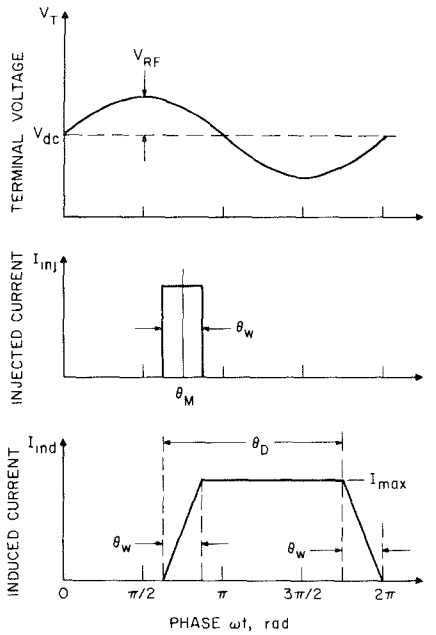


Fig. 1. Ideal voltage and current waveforms for a transit-time device.

down exist, and the TUNNETT (*tunnel transit-time*) mode, where pure tunneling is present.

## II. Simplified Analysis

### A. Voltage and Current Waveforms

Fig. 1 shows typical idealized voltage and current waveforms for the transit-time devices under consideration here, where $\theta_w$ is the injected current pulsewidth and $\theta_M$ is at the center of the pulse. $\theta_D$ is the drift region transit angle. The dc current is

$$I_{dc} = \frac{1}{2\pi}\int_0^{2\pi} I_{inj}\, d(\omega t) = \frac{1}{2\pi}\int_0^{2\pi} I_{ind}\, d(\omega t) \tag{1}$$

where $I_{inj}$ and $I_{ind}$ are the injected and induced currents, respectively. Therefore, the maximum induced current becomes

$$I_{max} = \left(\frac{2\pi}{\theta_D}\right) I_{dc}. \tag{2}$$

The dc power is

$$P_{dc} = V_{dc} I_{dc}. \tag{3}$$

The RF power is

$$P_{RF} = \frac{1}{2\pi}\int_0^{2\pi} I_{ind}(\omega t)\, V_{RF} \sin(\omega t)\, d(\omega t) \tag{4}$$

which simplifies to

$$P_{RF} = V_{RF} I_{dc} \left(\frac{\sin(\theta_w/2)}{(\theta_w/2)}\right) \cdot \left(\frac{\cos\theta_M - \cos(\theta_M + \theta_D)}{\theta_D}\right). \tag{5}$$

The device efficiency is

$$\eta \triangleq \frac{P_{RF}}{P_{dc}} = \left(\frac{V_{RF}}{V_{dc}}\right)\left(\frac{\sin(\theta_w/2)}{(\theta_w/2)}\right) \cdot \left(\frac{\cos\theta_M - \cos(\theta_M + \theta_D)}{\theta_D}\right). \tag{6}$$

$\theta_M$ and $\theta_w$ result primarily from the device design of the generation region, as will be shown later, and this will determine the particular mode of operation. For IMPATT mode operation, $\theta_M \cong \pi$, and (6) reduces to

$$\eta = \left(\frac{V_{RF}}{V_{dc}}\right)\left(\frac{\sin(\theta_w/2)}{\theta_w/2}\right)\left(\frac{\cos\theta_D - 1}{\theta_D}\right). \tag{7}$$

It can be seen from this equation that the larger $\theta_w$ is, the lower the efficiency. The best efficiency is obtained for $\theta_w = 0$. For this case

$$\eta = \left(\frac{V_{RF}}{V_{dc}}\right)\left(\frac{\cos\theta_D - 1}{\theta_D}\right) \tag{8}$$

and for $\theta_D = \pi$

$$\eta = -\frac{2}{\pi}\left(\frac{V_{RF}}{V_{dc}}\right). \tag{9}$$

The maximum efficiency for this case is obtained for $\theta_D = 0.74\pi$ where

$$\eta = -\frac{2.27}{\pi}\left(\frac{V_{RF}}{V_{dc}}\right). \tag{10}$$

In this mode of operation, $\theta_w$ decreases as the generation region width $x_g$ is decreased.

For TUNNETT mode operation, where $x_g$ is very small, $\theta_M \cong \pi/2$ and for $\theta_w = 0$, (6) becomes

$$\eta = \left(\frac{V_{RF}}{V_{dc}}\right)\left(\frac{\sin\theta_D}{\theta_D}\right). \tag{11}$$

The optimum generation efficiency is obtained for $\theta_D = 3\pi/2$ where

$$\eta = -\frac{2}{3\pi}\left(\frac{V_{RF}}{V_{dc}}\right). \tag{12}$$

It is, therefore, obvious that this mode will result in lower efficiency than the IMPATT mode but hopefully the noise would be much lower. Equation (6) also indicates that the efficiency would be maximum when $\theta_w \cong 0$, $\theta_M = 3\pi/2$, and $\theta_D = 0$. For this case

$$\eta = -\left(\frac{V_{RF}}{V_{dc}}\right). \tag{13}$$

For MITATT mode operation, $\pi/2 < \theta_M < \pi$; thus the efficiency in this mode will lie between the IMPATT and TUNNETT modes and so would the noise performance. $\theta_D$ is dependent on the device design of the drift region and for optimum performance, the following relationship is chosen such that at the frequency range of interest

$$\theta_M + (\theta_w/2) + \theta_D \cong 2\pi. \tag{14}$$

It will be shown later that the primary effect of increasing the operating frequency of the device is to increase $\theta_w$ which results in a smaller device efficiency. The tunnel

current in general lowers the RF power and device efficiency and at the same time improves the noise performance. The tunnel current also has an important effect on $\theta_w$ at high frequencies as will be shown later.

### B. Frequency Scaling Relations

Approximate frequency scaling relations can be derived from simple principles. The dc current density could be scaled as [6] $J_{dc} \propto f$ if space-charge effects are considered, or as $J_{dc} \propto f^2$ if the ratio of the operating frequency to the avalanche frequency is considered. Experimental results seem to indicate that the scaling is between these two relations. The dc voltage is scaled as $V_{dc} \propto 1/f$, and since $(V_{RF}/V_{dc})$ is usually about constant at the maximum efficiency point, it is found that $V_{RF} \propto 1/f$. The device conductance per unit area is proportional to $(J_{dc}/V_{RF})$ so $G_{dev} \propto f^2$ or $f^3$ depending on whether $J_{dc}$ is proportional to $f$ or $f^2$, respectively. The device susceptance per unit area is scaled as $B_{dev} \propto f^2$. Assuming the smallest microwave circuit resistance that it is possible to match into the device is $R_L^{min}$ yields a maximum area which is approximately

$$A_{max} = \frac{G_{dev}}{R_L^{min} B_{dev}^2} \tag{15}$$

which scales as $A_{max} \propto 1/f^2$ or $1/f$ if $R_L^{min}$ is constant as a function of frequency. Since the RF power is given as

$$P_{RF} = J_{dc} V_{dc} A_{max} \eta \tag{16}$$

the RF power is scaled as $P_{RF} \propto 1/f^2$ or constant if $\eta$ is constant as a function of frequency. At high frequencies, it is generally useful to scale $\eta \propto 1/f$ such that the RF power is scaled as $P_{RF} \propto 1/f^3$ or $1/f$. If thermal considerations are also included, the maximum temperature rise is given as

$$\Delta T_{max} = R_T P_{dc}(1-\eta) \tag{17}$$

where the thermal resistance is assumed to be dominated by the spreading resistance such that $R_T \propto 1/\sqrt{A_{max}}$. Assuming that $\eta \ll 1$, then (17) yields $P_{RF} \propto \eta\sqrt{A_{max}}$ such that the RF power is scaled as $P_{RF} \propto 1/f$ or $1/\sqrt{f}$ if $\eta$ is constant or as $P_{RF} \propto 1/f^2$ or $1/f^{3/2}$ if $\eta$ varies as $1/f$. Therefore, the frequency scaling relation that is applicable to $P_{RF}$ depends on what assumptions are made with regard to the scaling of $J_{dc}$ and $\eta$ and whether the thermal or circuit limitations dominate.

## III. Generation Region Large-Signal Analysis

### A. Calculation Method

The governing differential equation for the injected current density is given as [19], [20]

$$\tau_i^* \frac{d}{dt} J_{inj}(t) = (\alpha^* x_g - 1) J_{inj}(t) + J_{s_0} + J_T^* \tag{18}$$

where $J_{inj}$ is the injected current density and $J_{s_0}$ is the dc saturation current density. The generation region field $E_M(t)$ is assumed to be spatially constant but time varying. Calculations are given for two different intrinsic response time [21] relations of

$$\tau_i^* = \tau_g/2 \tag{19}$$

and [20]

$$\tau_i^* = \left(\frac{M_{a_0} - 1}{M_{a_0}}\right)\kappa_A \tau_g + \left(\frac{1}{M_{a_0}}\right)\tau_T^*. \tag{20}$$

The first relation is the simple result of a standard derivation where $\tau_g$ is the average transit time of the generation region. The second relation is a phenomenological equation where the first term is applicable to the IMPATT mode and the second term is applicable to the TUNNETT mode. $M_{a_0}$ is the avalanche multiplication factor [18]. The first term of (20) was motivated by the fact that in order to match experimental and theoretical admittance results for GaAs [22], $\tau_i^*$ was assumed to be larger than is indicated by (19). The second term of (20) was motivated by the assumption that tunneling has a very small response time $\tau_T^*$ which is not related to the avalanche process. For the purposes of this study the following values are used [19]: $\kappa_A^{GaAs} \sim (3/2)$, $\kappa_A^{Si} \sim (1/2)$, and $\tau_T^* \sim 10^{-14}$ s. $\alpha^*$ is the effective ionization rate which is influenced by "dead spaces" in very thin generation regions [19], [20], and approximate calculation methods are given elsewhere [20]. $J_T^*$ is the tunnel current density. Both $\alpha^*$ and $J_T^*$ are functions of $E_M(t)$ and $x_g$.

The injected current pulse is calculated by assuming that the generation region voltage is

$$V_g(t) \triangleq E_M(t) x_g = V_{g_b} + V_{g_{RF}} \sin(\omega t) \tag{21}$$

where $V_{g_b}$ is the bias voltage and $V_{g_{RF}}$ is the magnitude of the RF voltage in the generation region. Equation (18) is solved by using (21) along with the constraints that the average of $J_{inj}(t)$ over one RF cycle is equal to the dc current density $J_{dc}$ and that $J_{inj}(t)$ is periodic over one RF cycle. A Runge–Kutta-type numerical method was used and details are given elsewhere [19], [23]. The input parameters for the computer program are $f$, $V_{g_{RF}}$, $J_{dc}$, and $x_g$. The output parameters are $V_{g_b}$, $\theta_M$, $\theta_w$, and a table of values of $J_{inj}$ as a function of phase angle, where $\theta_M$ is the phase angle of maximum injected current density and $\theta_w$ is the phase angle width in which 80 percent of the injected charge is contained in the pulse.

### B. Results for GaAs and Si

The calculation method developed yields very efficient calculation of the large-signal injected current pulse for a diode in mixed avalanche-tunnel breakdown when the generation region is isolated from drift region effects. It is useful to study the generation region in isolation since the large-signal behavior of the drift region has been extensively studied [24]. This facilitates interpretation of the complete large-signal simulation of the device when there is interaction between the generation and drift regions.

Fig. 2 shows $J_{inj}$ as a function of phase angle for a Si diode in the MITATT mode where $\theta_M = 137°$ and $\theta_w = 47°$. The pulse is periodic with the correct average value and where the tunneling current causes $\theta_M$ to be less than

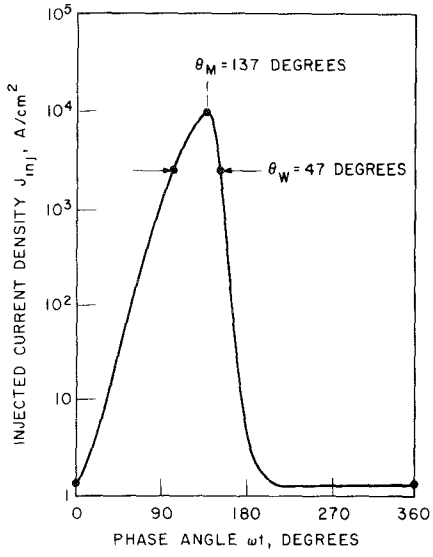


Fig. 2. Injected current density as a function of phase angle (Si, $x_g = 500$ A, $J_{dc} = 1000$ A/cm$^2$, $T = 300$ K, $f = 10$ GHz, $V_{g_{RF}} = 1.0$ V, $V_{g_0} = 7.59$ V, $V_{g_b} = 6.98$ V, and $M_{a_0} = 310$).

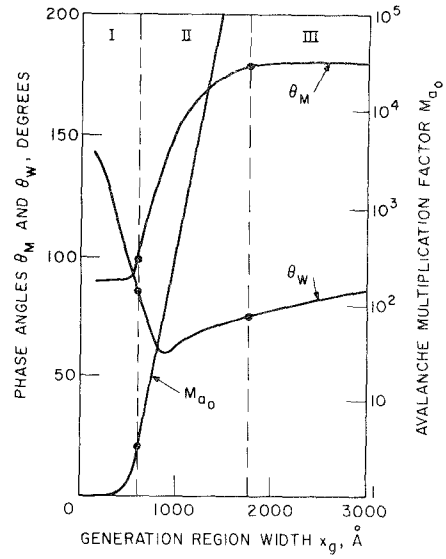


Fig. 4. Phase angles $\theta_M$ and $\theta_w$ and the avalanche multiplication factor $M_{a_0}$ as a function of generation region width [23] (GaAs, $J_{dc} = 1000$ A/cm$^2$, $T = 300$ K, $f = 10$ GHz, and $V_{g_{RF}} = 0.1 V_{g_0}$).

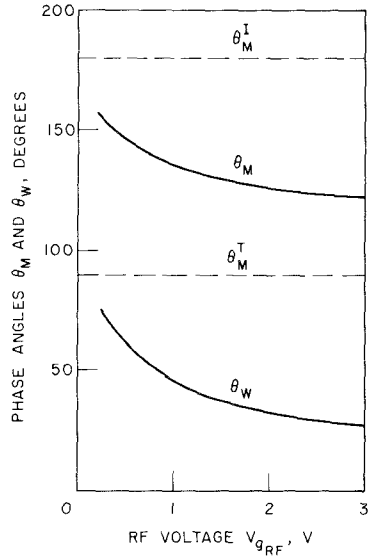


Fig. 3. Phase angles $\theta_M$ and $\theta_w$ as a function of RF voltage (Si, $x_g = 500$ A, $J_{dc} = 1000$ A/cm$^2$, $T = 300$ K, $f_{RF} = 10$ GHz, $V_{g_0} = 7.59$ V, and $M_{a_0} = 310$).

180°. The effect of $V_{g_{RF}}$ on $\theta_M$ and $\theta_w$ is shown in Fig. 3 for the same Si device. $\theta_M$ decreases as $V_{g_{RF}}$ increases. This is caused by $J_{inj}$ ($\theta = 0$) decreasing, at large RF drives, to the point where it is comparable to $J_T^*$ such that the tunneling current affects the injected current buildup more at large RF drives. The superscripts $I$ and $T$ on $\theta_w$ indicate the ideal values that occur for pure avalanche and pure tunneling, respectively. The MITATT mode, therefore, displays increasing tunnel effects as the RF drive increases. It should be noted that space-charge effects in the drift region tend to dominate this effect such that $\theta_M$ will increase slightly as the RF drive is increased. $\theta_w$ also decreases as $V_{g_{RF}}$ increases which, as indicated by (6), will increase the device efficiency.

The injected current pulse is greatly affected by the relative strength of the tunnel current, which is controlled by the device structure parameter $x_g$ and is given numerical significance in the parameter $M_{a_0}$. The effect of $x_g$ on $\theta_M$ and $\theta_w$ is shown in Fig. 4 for a GaAs diode where $M_{a_0}$ is also plotted. Notice that as $x_g$ increases, the breakdown becomes avalanche dominated and, consequently, $M_{a_0}$ increases which results in $\theta_M$ increasing; $\theta_w$ at first decreases but then increases. All these trends are expected from physical considerations. The regions of $x_g$ labeled I, II, and III designate the three distinct modes of operation named TUNNETT, MITATT, and IMPATT, respectively. From (6), $\eta$ will increase as $\theta_M$ increases or as $\theta_w$ decreases. It is interesting to note that the minimum $\theta_w$ occurs in the MITATT range and the corresponding $\theta_M$ is not greatly below 180°, which indicates that the device efficiency will not be greatly degraded by moderate tunnel currents and the noise performance should be greatly improved.

It is believed by the authors that an important effect which leads to the high-frequency limitations of IMPATT mode devices is to be found in the dynamics of the injected current pulse formation. Since $\theta_M$ and $\theta_w$ characterize the pulse, it is very informative to study the two phase angles as a function of frequency, device structure, and device material. Fig. 5 shows $\theta_w$ as a function of frequency for three GaAs diode structures where $(V_{g_{RF}}/V_{g_0})$ and $J_{dc}$ are held constant. The generation region widths chosen were $x_g = 500$, 1000, and 2000 Å which achieve device operation in the TUNNETT, MITATT, and IMPATT modes, respectively. The results shown were calculated for both of the intrinsic response time relations as given in (19) and (20). For GaAs, the two expressions for $\tau_i^*$ yield greatly differing results. The half transit-time approximation for $\tau_i^*$ always gives a much smaller $\theta_w$ than the phenomenological equation for $\tau_i^*$. Notice that $\theta_w$ increases rapidly as the frequency increases for IMPATT mode devices, but as the amount of tunneling increases, $\theta_w$ increases much less rapidly as the

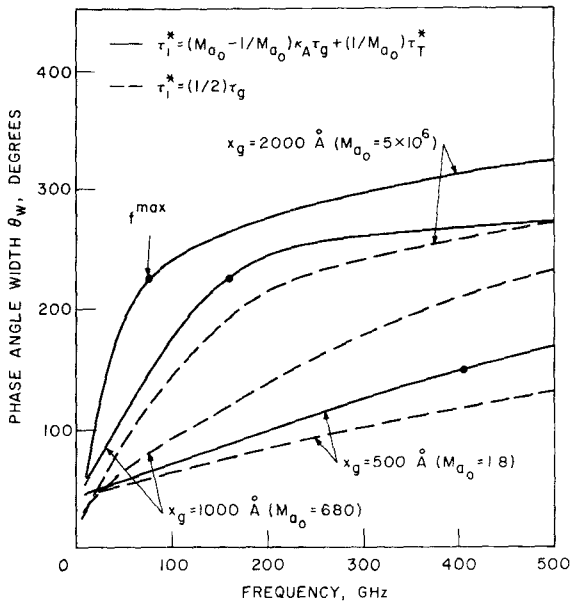


Fig. 5. Phase angle width as a function of frequency for various generation region widths and two different intrinsic response time relations (GaAs, $J_{dc} = 1000$ A/cm$^2$, $T = 300$ K, $V_{g_{RF}} = 0.5V_{g_0}$).

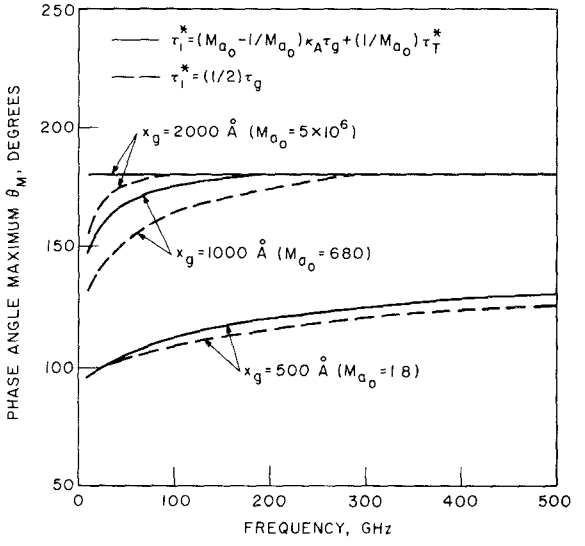


Fig. 6. Phase angle maximum as a function of frequency for various generation region widths and for two different intrinsic response time relations (GaAs, $J_{dc} = 1000$ A/cm$^2$, $T = 300$ K, and $V_{g_{RF}} = 0.50V_{g_0}$).

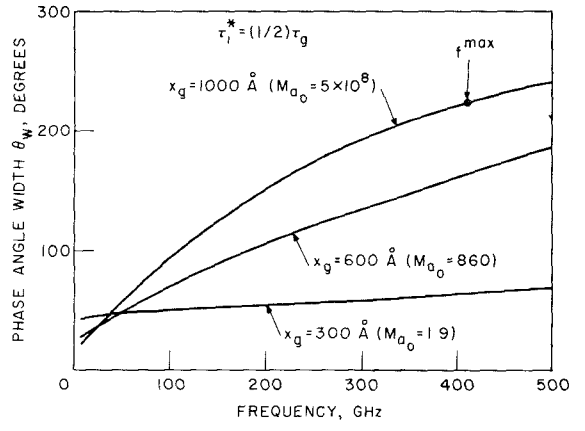


Fig. 7. Phase angle width as a function of frequency for various generation region widths (Si, $J_{dc} = 1000$ A/cm$^2$, $T = 300$ K, and $V_{g_{RF}} = 0.50V_{g_0}$).

frequency increases. In order to estimate the high-frequency limitations of each mode of operation, in a given semiconductor material, a maximum frequency is defined by

$$\theta_w(f^{max}) \triangleq 1.25 \lim_{f \to 500\text{ GHz}} \theta_M \qquad (22)$$

and is represented by a dot on the $\theta_M$–$f$ profiles shown in Fig. 5. Equation (22) was developed by consideration of physical principles, experimental data of state-of-the-art performance in IMPATT diodes, experience with a large-signal simulation of transit-time diodes [5], and (6). Using the results calculated on the basis of the phenomenological equation for $\tau_i^*$ in Fig. 5, which is believed to be a better relation than (19), yields $f^{max}$ of 75, 150, and 400 GHz for the IMPATT, MITATT, and TUNNETT modes, respectively, in GaAs. The $f^{max}$ of GaAs IMPATT mode devices is small due to the rather long time needed to build up carriers by successive impact ionizations, which may necessitate scattering between conduction bands [4]. What is very interesting is that tunneling can greatly increase $f^{max}$ and this factor will allow fabrication of GaAs devices which operate at much higher frequencies. Higher frequency operation can possibly also be obtained in GaAs devices by changing the crystallographic orientation of the active region since the ionization rates change in different crystal directions [25]. Fig. 6 shows $\theta_M$ as a function of frequency for the same three GaAs diode structures. What should be noted is that both IMPATT and MITATT mode devices have $\theta_M \to \theta_M^I = 180°$ at high frequencies and that $\theta_M$ becomes greater than $\theta_M^T = 90°$ for TUNNETT mode devices at high frequencies. Fig. 7 shows $\theta_w$ as a function of frequency for IMPATT, MITATT, and TUNNETT mode Si devices where $J_{dc}$ and $(V_{g_{RF}}/V_{g_0})$ are held constant. For Si, either expression for $\tau_i^*$ yields essentially identical results. What is very noticeable is that Si has much better high-frequency performance than GaAs. From Fig. 7, $f^{max}$ is calculated to be 400, >500, and >500 GHz for the IMPATT, MITATT, and TUNNETT modes, respectively, in Si. Notice that $[f^{max}]^I_{Si} \sim 5[f^{max}]^I_{GaAs}$ and that tunneling for both GaAs and Si devices greatly extends the upper frequency limit of operation. Fig. 8 shows $\theta_M$ as a function of frequency for the same three Si diode structures. The results are similar to the results shown in Fig. 6 for GaAs.

## IV. Large-Signal Diode Simulations

### A. Brief Description of Computer Model

In order to test the predictions of the previous section, results are presented in this section which are based on computations employing a complete device simulation program which is described elsewhere [19], [23]. The device simulation assumes a $p^+$-i-$n^+$-n(x)-$n^+$ (low–high–general) doping profile. The generation region is modeled

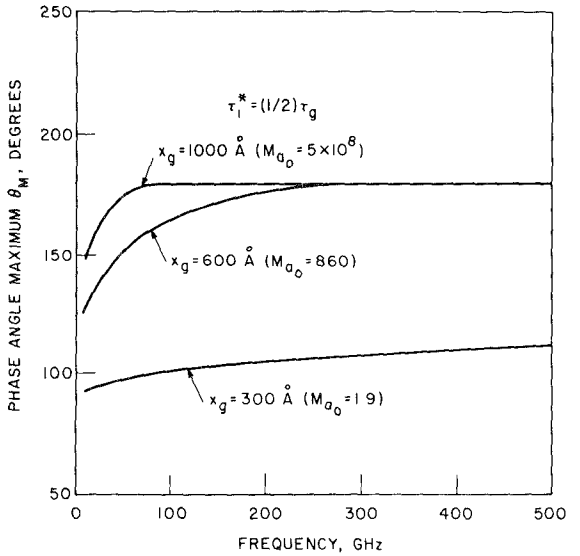


Fig. 8. Phase angle maximum as a function of frequency for various generation region widths (Si, $J_{dc} = 1000$ A/cm$^2$, $T = 300$ K, and $V_{g_{RF}} = 0.50 V_{g_0}$).

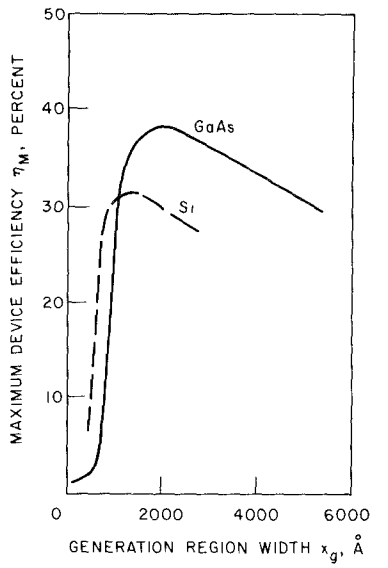


Fig. 9. Maximum device efficiency as a function of generation region width for GaAs and Si low–high–medium $X$-band devices [23].

as described in the previous section and the drift region is modeled by use of difference equation versions of the device equations where the carrier velocities, diffusion coefficients, and ionization rates are field dependent. The model assumes a constant field and no space-charge effects in the generation region which is a basic limitation of the model, but it is also useful since the intrinsic response time can be easily adjusted. DC and large-signal results are efficiently obtained from this model where the input parameters are $J_{dc}$, $V_{RF}$, $f$, $x_g$, $w$, and the doping profile. The computer program calculates many dc and large-signal parameters which include the device conductance $G_{dev}$, the device susceptance $B_{dev}$, and the efficiency $\eta$.

### B. Results for GaAs and Si

Fig. 9 shows directly the effect of the tunneling current on GaAs and Si low–high–medium $X$-band devices. The maximum efficiency, which is found by optimizing over the parameters $V_{RF}$ and $f$, at $J_{dc} = 1000$ A/cm$^2$ is shown as a function of $x_g$. The devices studied have a drift region width of 5 $\mu$m with a punchthrough factor of one. For small $x_g \leqq 700$ Å, in GaAs, the devices operate in the TUNNETT mode and $\eta_M \leqq 6$ percent which is as expected. For large $x_g \geqq 2000$ Å, in GaAs, the devices operate in the IMPATT mode where $\eta_M$ reaches a maximum of 38 percent and $\eta_M$ decreases as $x_g$ increases due to $\theta_w$ increasing. For 700 Å $< x_g <$ 2000 Å, in GaAs, the devices operate in the MITATT mode, where $\eta_M$ increases due to $\theta_M$ increasing as $x_g$ increases. Results are also shown for Si devices. It is interesting to note that in a GaAs MITATT mode device with $x_g = 1000$ Å, $\eta_M$ is equal to 26 percent and since $M_{a_0}$ is equal to 700 this should be a much less noisy device than the IMPATT mode device.

A study was also conducted on similar low–high–medium diode structures which were designed to approximate the high-frequency performance of uniformly doped diode structures. The electric field profile of the "quasi-uniform" diode structure is shown in Fig. 10. Using a more general device simulation has shown that the performance of the quasi-uniform structure is similar to the uniform structure except that the device efficiency is smaller in the quasi-uniform structure [19]. To increase the operating frequency of the device, $w$ is decreased and details of the device design are given elsewhere [19]. The current density is scaled as $J_{dc} \sim f^2$ and the punchthrough factor is one for all devices. The results of the quasi-uniform study for Si and GaAs devices are also compared to results obtained from TUNNETT and MITATT mode, GaAs, Read-type diode structures at high frequencies. Many $G$–$B$ and $\eta$–$V_{RF}$ profiles were generated [19] for various device structures. Fig. 11 shows a typical $\eta$–$V_{RF}$ profile for a quasi-uniform, GaAs, 2-$\mu$m device where the intrinsic response time is calculated for both $(\frac{1}{2})\tau_g$ and

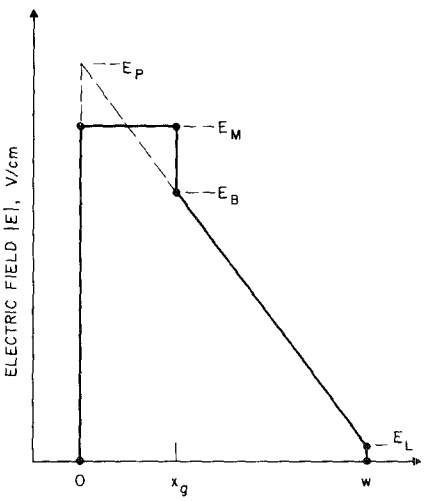


Fig. 10. Electric field profile for the quasi-uniform device structure.

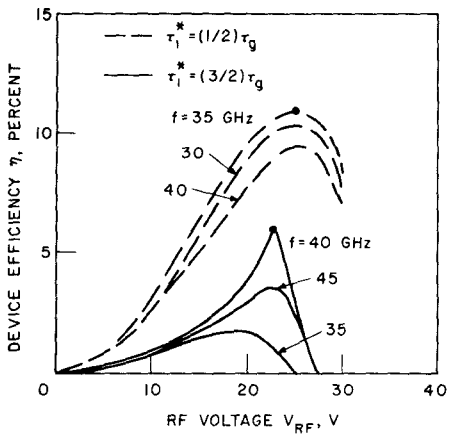


Fig. 11. Device efficiency as a function of RF voltage for various frequencies and for two different intrinsic response time relations (GaAs, $w = 2$ μm, and $J_{dc} = 10\,000$ A/cm$^2$).

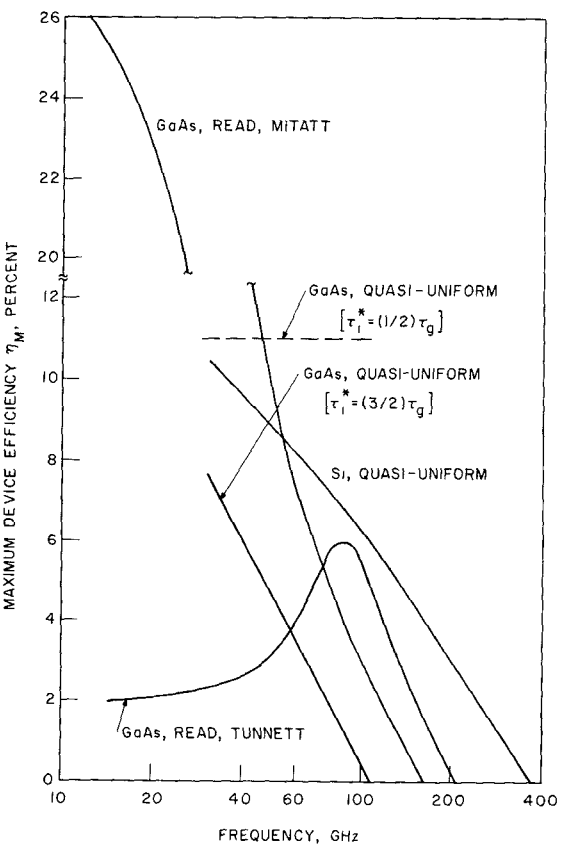


Fig. 12. Maximum device efficiency as a function of frequency for Si quasi-uniform, GaAs quasi-uniform, and GaAs Read TUNNETT and MITATT devices.

$(\frac{3}{2})\tau_g$. Notice that as $\tau_i^*$ increases $\eta_M$ decreases and the frequency of operation shifts upward. This is expected since the injected current pulse cannot form well at this frequency as $\tau_i^*$ is increased to $(\frac{3}{2})\tau_g$. $\tau_i^* = (\frac{3}{2})\tau_g$ was used at $X$ band in order to match experimental and theoretical $G$–$B$ data [22] for GaAs devices. The complete study is summarized in Fig. 12 where $\eta_M$ is shown as a function of frequency for the devices simulated. For Si quasi-uniform devices $\eta_M$ decreases with frequency since $\theta_w$ is increasing,

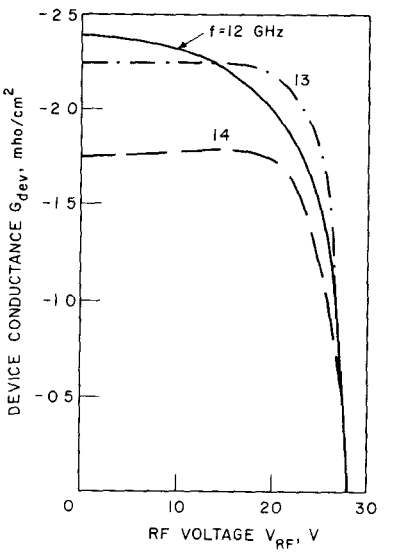


Fig. 13. Device negative conductance as a function of RF voltage for various frequencies (GaAs, $w = 5$ μm, $x_g = 200$ Å, and $J_{dc} = 1000$ A/cm$^2$).

and the maximum frequency in which large-signal negative conductance is achieved is $f_{LS}^{max} = 350$ GHz which corresponds well with experimental results and the predictions of the generation region analysis of the last section. For GaAs quasi-uniform structures with $\tau_i^* = (\frac{3}{2})\tau_g$, $\eta_M$ decreases with frequency and $f_{LS}^{max} = 100$ GHz which is consistent with experimental results for GaAs IMPATT diodes. The results shown for GaAs quasi-uniform structures with $\tau_i^* = (\frac{1}{2})\tau_g$ indicate that $f_{LS}^{max} > 100$ GHz which is contrary to experimental evidence. Therefore, the use of $\tau_i^* = (\frac{3}{2})\tau_g$ yields both the correct correlation between experimental and theoretical $G$–$B$ results [22] and also substantiates the fact that little success has been achieved with high-frequency GaAs diodes in the low millimeter-wave frequency range. For GaAs Read-type TUNNETT mode structures, $\eta_M$ at first increases with frequency up to 6 percent at 100 GHz and then decreases with frequency with $f_{LS}^{max} = 200$ GHz. $\eta_M$ starts out increasing with frequency because the generation region can achieve greater voltage modulation, before avalanche multiplication occurs in the drift region, as the drift region voltage approaches the generation region voltage since $\theta_w$ decreases as $V_{g_{RF}}$ increases. Since the TUNNETT should be a very quiet device, a 100-GHz device with 6-percent efficiency and low noise would be a very useful device. For GaAs Read-type MITATT mode devices, $\eta_M$ decreases as a function of frequency and $f_{LS}^{max} = 150$ GHz which is between the IMPATT mode and TUNNETT mode cases. Therefore, this study has indicated that Si devices have a fundamental larger high-frequency limit than GaAs devices and in GaAs, tunneling effects can greatly improve high-frequency performance.

The TUNNETT should also be useful as a low-noise amplifier particularly at millimeter wavelengths. A typical device conductance versus $V_{RF}$ for a typical $X$-band TUNNETT device is shown in Fig. 13. These results

indicate that a TUNNETT device can be used effectively as a low-noise amplifier with a large dynamic range.

## V. Conclusions

The high-frequency limitations of IMPATT, MITATT, and TUNNETT mode devices were explored by concentrating on the details of the large-signal injected current pulse formation. A simple relation for the device efficiency was given and various approaches to the "scaling laws" were also included. Large-signal results were given for GaAs and Si devices both for a model of the generation region and for a model of the total device. The first model showed how the pulsewidth was affected by tunneling and by frequency and estimates were made for the high-frequency limitations of GaAs and Si devices. The second model showed how the device efficiency was affected by tunneling and by frequency and again the high-frequency limitations of GaAs and Si devices were given. In general, Si devices have been shown to have a larger high-frequency limit than GaAs devices and in GaAs, tunneling effects can greatly improve high-frequency performance. It was also shown that a very quiet TUNNETT mode device can be constructed at 100 GHz in GaAs with a predicted efficiency of 6 percent.

It is believed that MITATT and TUNNETT mode devices will be extremely useful as low-noise amplifiers, oscillators, self-oscillating mixers, and detectors particularly at millimeter wavelengths. Some preliminary experimental results have been obtained recently which are worth noting here [26].

## References


[1] B. C. DeLoach, Jr., "Thin skin IMPATTS," *IEEE Trans. Microwave Theory Tech.*, vol. MTT-18, pp. 72–74, Jan. 1970.

[2] M. S. Gupta, "A simple approximate method of estimating the effect of carrier diffusion in IMPATT diodes," *Solid-State Electron.*, vol. 18, pp. 327–330, 1975.

[3] R. Schwarz, H. W. Thim, and H. W. Potzl, *Electron. Lett.*, vol. 13, pp. 288–289, May 12, 1977.

[4] R. Kuvås and C. A. Lee, "Carrier diffusion in semiconductor avalanches," *J. Appl. Phys.*, vol. 41, pp. 3108–3116, June 1970.

[5] T. Misawa, "High-frequency fall-off of IMPATT diode efficiency," *Solid-State Electron.*, vol. 15, pp. 457–465, 1972.

[6] D. L. Scharfetter, "Power-impedance-frequency limitations of IMPATT oscillators calculated from a scaling approximation," *IEEE Trans. Electron Devices*, vol. ED-18, pp. 536–543, Aug. 1971.

[7] G. Gibbons, J. J. Purcell, P. R. Wickens, and H. S. Gokgor, "50 GHz gallium arsenide IMPATT oscillator," *Electron. Lett.*, vol. 8, pp. 513–514, 19, Oct. 1972.

[8] M. Ohmori, T. Ishibashi, and S. Ono, "Dependency of the highest harmonic oscillation frequency on junction diameter of IMPATT diodes," *IEEE Trans. Electron Devices*, vol. ED-24, pp. 1323–1329, Dec. 1977.

[9] L. S. Bowman and C. A. Burrus, Jr., "Pulse-driven silicon p-n junction avalanche oscillators for the 0.9 to 20 mm band," *IEEE Trans. Electron Devices*, vol. ED-14, pp. 411–418, Aug. 1967.

[10] A. G. Chynoweth and K. G. McKay, "Internal field emission in silicon p-n junctions," *Phys. Rev.*, vol. 106, pp. 418–426, May 1, 1957.

[11] H. Weinerth, "Silicon diode breakdown in the transition range between avalanche effect and field emission," *Solid-State Electron.*, vol. 10, pp. 1053–1062, Nov. 1967.

[12] M. Singh Tyagi, "Zener and avalanche breakdown in silicon alloyed p-n junctions," *Solid-State Electron.*, vol. 11, pp. 99–115, Jan. 1968.

[13] W. A. Lukaszek, A. van der Ziel, and E. R. Chenette, "Investigation of the transition from tunneling to impact ionization multiplication in silicon p-n junctions," *Solid-State Electron.*, vol. 19, pp. 57–71, Jan. 1976.

[14] A. Semichon, J. Michel, E. Constant, and A. Vanoverschelde, "Microwave oscillation of a tunnel transit-time diode," in *Proc. 8th Int. Conf. on Microwaves and Optical Generation and Amplification* (Amsterdam, The Netherlands), pp. 7-15–7-20, Sept. 1970.

[15] J. Nishizawa, T. Ohmi, and T. Sakai, "Millimeter-wave oscillations from TUNNETT diodes," in *Proc. European Microwave Conf.* (Paris, France), pp. 449–453, Sept. 1974.

[16] S. P. Kwok and G. I. Haddad, "Effects of tunneling on an IMPATT oscillator," *J. Appl. Phys.*, vol. 43, pp. 3824–3830, Sept. 1972.

[17] M. Chive, E. Constant, M. Lefebvre, and J. Pribetich, "Effect of tunneling on high-efficiency IMPATT avalanche diodes," *Proc. IEEE* (Lett.), vol. 63, pp. 824–826, May 1975.

[18] M. E. Elta and G. I. Haddad, "Mixed tunneling and avalanche mechanisms in p-n junctions and their effects on microwave transit-time devices," *IEEE Trans. Electron Devices*, vol. ED-25, pp. 694–702, June 1978.

[19] M. E. Elta, "The effects of mixed tunneling and avalanche breakdown on microwave transit-time diodes," Tech. Rep. 142, Electron Physics Laboratory, Univ. of Michigan, Ann Arbor, June 1978.

[20] M. E. Elta and G. I. Haddad, "The calculation of effective ionization rates for p-n junctions with small generation region widths," *IEEE Trans. Electron Devices*, (to be published).

[21] R. Kuvås and C. A. Lee, "Quasistatic approximation for semiconductor avalanches," *J. Appl. Phys.*, vol. 41, pp. 1743–1755, Mar. 1970.

[22] C. A. Lee, J. Berenz, and G. C. Dalman, "Determination of GaAs intrinsic avalanche response time from noise measurements," in *Proc. 6th Biennial Cornell Electrical Engineering Conf.* (Ithaca, NY), pp. 233–245, Aug. 1977.

[23] M. E. Elta and G. I. Haddad, "Large-signal performance of microwave transit-time devices in mixed tunneling and avalanche breakdown," *IEEE Trans. Electron. Devices*, June 1979 (to be published).

[24] P. E. Bauhahn and G. I. Haddad, "IMPATT device simulation and properties," *IEEE Trans. Electron Devices*, vol. ED-24, pp. 634–642, June 1977.

[25] T. P. Pearsall, F. Capasso, R. E. Nahory, M. A. Pollack, and J. R. Chelikowsky, "The band structure dependence of impact ionization by hot carriers in semiconductors: GaAs," *Solid-State Electron.*, vol. 21, pp. 297–302, 1978.

[26] J. Nishizawa, K. Motoya, and Y. Okuno, "The GaAs TUNNETT diodes," in *IEEE MTT-S Int. Microwave Symp. Digest* (Ottawa, Canada), pp. 159–161, June 1978.